Long Range Ordering in Model Ni-Cr-X Alloys

George A. Young and Daniel R. Eno

Knolls Atomic Power Laboratory
Bechtel Marine Propulsion Corporation
Schenectady, NY 12309

*Corresponding Author: george.young@unnpp.gov

KEYWORDS: Long Range Order, Nickel-Chromium, Alloy 690, Ni_2Cr

Introduction

Nickel-chromium alloys are used throughout commercial nuclear power systems due to their desirable combination of corrosion resistance and mechanical properties. However, some Ni-Cr alloys can undergo long range ordering (LRO), forming the Ni_2Cr phase when exposed to temperatures < 590°C [1-3]. Long range ordering results in lattice contraction, hardening, and a change in slip mode, which, in turn, can cause dimensional changes, internal stress, and appreciable embrittlement [4-8]. Despite the technological importance of this alloy system, the variables that influence LRO are not well understood and the time-temperature-transformation kinetics poorly defined. In part, these limitations are due to the sluggish nature of the ordering reaction at low temperatures and to the metallurgical complexity of engineering alloys. In order to assess the risk of LRO in nuclear power systems, the present research uses model Ni-Cr alloys and ageing times up to 10,000 hours to define the kinetics of LRO and to assess the effects of cold work, quench rate, and alloying additions. Results show that the hardening caused by ordering is well described by the Kolomogorov-Johnson-Mehl-Avrami (KJMA) equation with an Avrami exponent, n ~0.65 and an apparent activation energy that depends on the starting condition of the alloy. Furnace cooled samples displayed a Q ~244 kJ/mol, which suggests bulk diffusional growth of the ordered phase, while water quenched samples exhibited a Q ~147 kJ/mol, indicating that excess vacancies accelerate ordering. Cold work (10% or 20%) acts to disrupt any ordering that forms on furnace cooling but has no apparent effect on the apparent activation energy or Avrami exponent. Iron additions decrease the temperature below which the ordered phase is stable but do not appear to affect the rate of ordering. Investigation of other alloying suggest that molybdenum (~2.47 wt.%) may accelerate ordering but other alloying elements studied (Si up to 0.28 wt.%, Mn up to 0.19 wt.%, and Nb up to 2.38 wt.%) have little influence. These findings, combined with a review of LRO in commercial alloys indicate that LRO can develop over a wide range of compositions and suggest that Alloy 690 is not immune to LRO. However, barring some accelerating factor, thermal ageing studies indicate LRO is only a concern for components exposed to high temperatures (≥325°C) for a decade or more.

Experimental Procedure

The alloys studied were fabricated with a Ni:Cr ratio near 2:1. In addition to the binary alloys, ternary and quaternary alloys with iron, silicon, manganese, and niobium were investigated, as well as 'model' versions of Alloy 690 and EN52i weld metal. Iron additions were investigated at 1, 3, 5, 7, and 9 atomic %, while the ternary and quaternary alloying additions were studied at a 'low' and 'high' level. The 'high' alloying level was chosen either to be near a common level in commercial alloys or for 1:1 comparison while the 'low' level was approximately 10X less than the 'high' concentration. For example, the Mn and Si levels are typical of commercial Alloy 690, the Nb concentration is near EN82 and EN52i weld metals, and Mo was chosen to match Nb.

The water quenched, furnace cooled, and cold worked conditions were investigated for times and temperatures given in Table 1. The degree of order was quantified via Vicker's microhardness testing (500 gf), building on previous research that used both x-ray diffraction and microhardness to assess ordering [9]. Additionally, the room temperature tensile properties and microstructure of selected binary samples were assessed.

	Ageing Time in Hours						
Temperature (°F / °C)	10	30	100	300	1,000	3,000	10,000
878 / 470	x	x	x	x	x	x	x
784 / 418		x	x	x	x	x	x
703 / 373			x	x	x	x	x
631 / 333				x	x	x	x

Table 1: **Ageing Times and Temperatures**

Material	Details
Ni-Cr Binary	Furnace cooled, water quenched Effects of cold work (10% and 20%)
Ternary and Quaternary Alloys	1, 3, 5, 7, 9% Fe, Fe + cold work, Fe with WQ and FC High and low levels of Nb, Mo, Si, Mn Combination of Mn+Si,
Model Alloys	Model Alloy 690 (Ni-Cr-Fe-Mn-Si) and EN52i (Ni-Cr-Mn-Nb-Fe)

Table 2: Alloys Additions to Ni_2Cr

Results and Discussion

Effect of LRO on Tensile Properties and Fracture Mode

The effect of ageing time at 475°C (887°F) on the tensile properties on a wrought Ni-330 at.% Cr alloy (i.e., Ni_2Cr) is given in Figure 1. The plot shows a marked increase in yield strength and decrease in tensile ductility (%RA) at ageing times ≥10 hours. The strength increase and ductility decrease saturate at approximately 500 hours. Looking at the extremes in the properties, LRO has produced a 2.5X increase in the yield strength (~200 to 500 MPa), and an 8X decrease in the ductility (~80% RA to ~10% RA). Note how the fracture mode changes from microvoid coalescence at short times (0-1 hours) to a less ductile mixed mode fracture ~200 hours, to purely intergranular fracture by 3000 hours. This dramatic increase in strength, decrease in ductility, and change in fracture mode highlights the concern for LRO developing in-service and degrading the toughness and likely the environmentally assisted cracking resistance of Ni-Cr alloys.

These changes in mechanical properties and fracture mode are solely attributable to the development of the Ni_2Cr ordered phase in this binary alloy. Both metallographic, SEM, and TEM indicate that the ordered phase is the only significant metallurgical change occurring in these alloys during isothermal ageing, as shown previously in Reference [8]. Figure 2 presents TEM evidence of LRO in a sample aged at 475°C (887°F) for 2000 hours, while Figure 3 shows good correlation between the increase in hardness with ageing and the increase in yield strength of the Ni-Cr binary alloys. These data support using hardness (or change in hardness) as an indicator of the development of LRO.

Compositions

The actual compositions of the alloys studied are given in Tables 1 and 2, with the values given in both weight percent and (atomic percent). As discussed, all of the alloys maintain a Ni:Cr ratio of approximately 2:1 (ranging from 1.87-2.19), in order to more clearly understand the effect of alloying elements. Most of the actual compositions were in good agreement with the target values with a few exceptions. For example the Ni-Cr-5Fe water quenched alloy was a little low in nickel, resulting in a Ni:Cr ratio of 1.87, the Ni-Cr-3Fe+20% CW alloys was high in nickel (Ni:Cr of 2.19), while the Ni-Cr-9Fe furnace cooled alloy was low in iron (~8 wt.%). For brevity, the target compositions of each alloy will be used in the discussion.

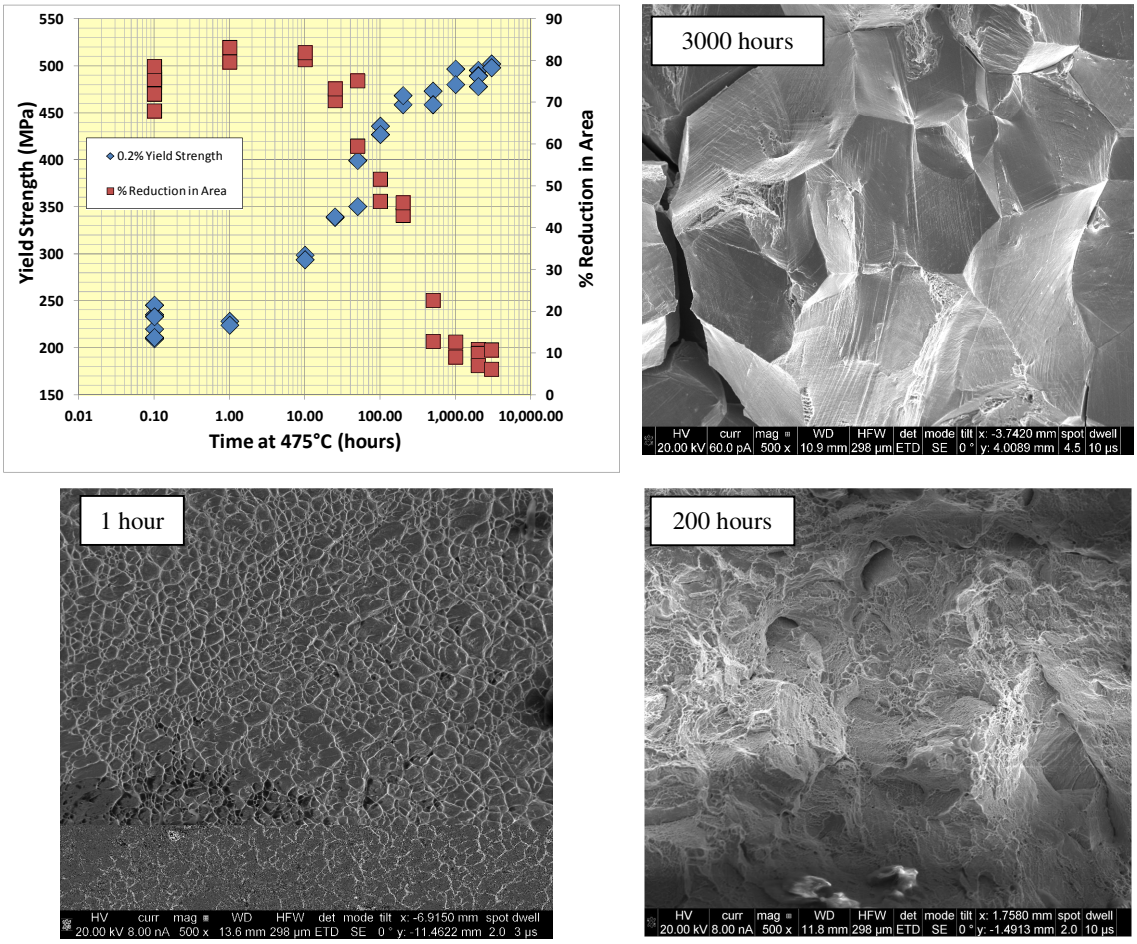

Figure 1: Effect of ageing at 475°C on the tensile properties and fracture mode of an Ni-33 at.% Cr alloy.

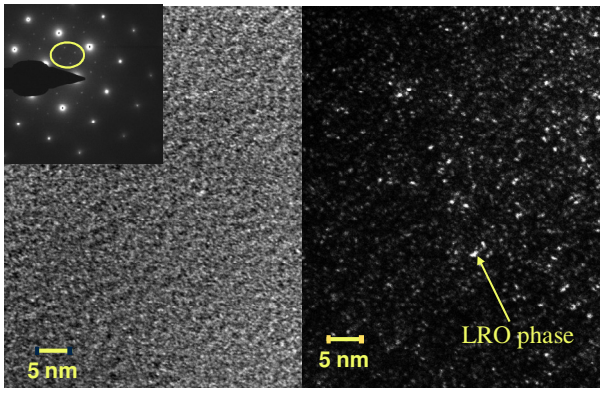

Figure 2. Brightfield / Darkfield image pair of a sample aged for 2000 hours at 475°C. The DF image formed along [100] zone axis using superlattice reflection from b = 1/3 ⟨220⟩ and shows clear evidence of long range order.

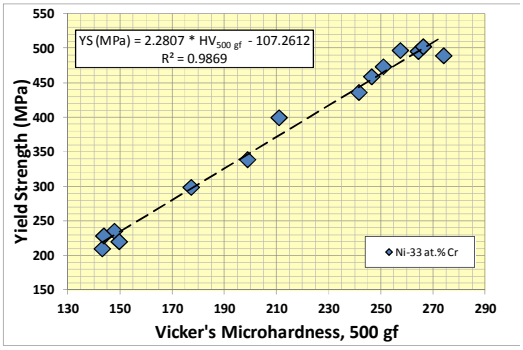

Figure 3: Correlation between the Vicker's microhardness number and the yield strength of a Ni-33 at.% Cr alloy. Isothermal ageing at 475°C (887°F) for up to 10,000 hours.

Curve Fitting

The microhardness data were fit to the Kolomogorov-Johnson-Mehl-Avrami (KJMA) equation [10-14] as per previous work with the JMP statistical software package. In the KJMA Equation (1), f is the fraction transformed, which is assumed to be directly proportional to the change in hardness value from the initial (un-aged) condition. The parameters H_0, H_{max}, and H are the initial, maximum, and instantaneous hardness values respectively, t is the ageing time in hours, and n, the 'Avrami exponent'. Additionally, k is assumed to have an Arrhenius form (Equation 2), where k_0 is a constant, Q the apparent activation energy, R is the gas constant, and T the absolute temperature (Kelvin) [8].

Unlike earlier work, there were sufficient data and understanding of the phenomena in this paper to test and group like datasets in order to better estimate the equation parameters [8]. Specifically, the binary, Ni-Cr-1Fe, and Ni-Cr-3Fe datasets, in both the furnace cooled and water quenched conditions were statistically analyzed. The cold worked data were excluded from this fitting, since the tendency for softening prior to hardening (LRO) in many of the data sets confounded fitting of the KJMA equation. Similarly, the higher iron alloys were excluded from the grouping since, for some temperatures, alloys with ≥ 5 at.% iron were at or beyond the critical temperature above which the LRO phase is stable [8].

$$f = \frac{(H - H_0)}{(H_{\max} - H_0)} = \left(1 - e^{-(kt)^n}\right) \quad (1)$$

Where k is assumed to have an Arrhenius form:

$$k = k_0 e^{-Q/RT} \quad (2)$$

Figure 4, shows the actual vs. predicted hardness curves for: (4a) all parameters adjustable (i.e., H_0, H_{max}, k_0, Q, and n), (4b) a single n, (4c) a single Q and n, and (4d) two Q's and a single n. The red points correspond to furnace cooled data and the blue points to water quenched data. The dashed lines represent "two-sigma" (approximately 95% coverage) bands around the best estimates, with the standard deviation (sigma) estimated from model (4d). There is no statistically significant difference between (4a) and (4b), indicating that a single n is justified. Forcing a single Q (4c) makes the fit significantly worse than (4a) so that two Q's seems and one n (4d) is judged to be the most reasonable and physically justifiable model, i.e., excess vacancies in the WQ material lower the apparent activation energy.

Binary Alloys

Results from the nickel-chromium binary alloys are summarized in Figure 5. Note that the range of the hardness values on the y-axis is the same for each condition (Δ=160 HV) to facilitate comparison of materials with different starting hardness values. As discussed, the KJMA fits utilize a common Avrami exponent of n~0.65, which indicates diffusion controlled growth between one dimension (n=0.5) and two dimensions (n=1) [15]. This is consistent with available literature studies that suggest asymmetrical growth of the ordered phase as elongated disks [16].

In the first comparison (left hand column), the water quenched alloy shows a markedly lower apparent activation energy (~147 kJ/mol (+17/-16 kJ/mol with 95% confidence)) than the furnace cooled alloy (~244 (+21/-19 kJ/mol with 95% confidence)). This is illustrated by the smaller spacing between the curve fits (dashed lines) between the WQ alloy (bottom left plot) than the furnace cooled alloy (top left). Note that the ageing temperatures were selected to be evenly spaced in reciprocal absolute temperature. The difference in apparent activation energy indicates that with excess vacancies, the ordering rate is governed by vacancy hopping Q ~135 kJ/mol) [17]. In contrast, the furnace cooled samples (i.e., thermal equilibrium vacancies) show an apparent activation energy closer to bulk diffusion (e.g. Cr diffusion in Ni is ~273 kJ/mol) in good agreement with other kinetics studies that show bulk diffusion governs ordering rates under conditions near thermal equilibrium [18, 19].

The right hand column of Figure 5 shows the hardening of the 10% (top) and 20% (bottom) cold worked alloys. Note that these data are fitted with the same Q (244 kJ/mol) and Avrami exponent as the non-cold worked, furnace cooled alloy but with a different k_0. This comparison shows that cold work acts to delay the onset of ordering, likely by destroying any order that forms on furnace cooling but does not significantly affect the ordering rate, once the process has begun. Note that the curve fits to the water quenched and furnace cooled binary alloys are used in several subsequent graphs in order to assess if alloying additions promote or delay the ordering kinetics.

Alloy	Condition[5]	Wt.% (At.%) [1, 2]												Atomic Ni:Cr
		Ni	Cr	Fe	Cu	Nb	Ti	Si	W	C[3]	O[4]	P	S[3]	
Ni-Cr	**FC**	69.72 (68.18)	30.25 (31.76)	<0.01 ---	0.02 (0.02)	<0.01 ---	<0.01 ---	<0.01 ---	<0.01 ---	0.008 (0.036)	0.002 (0.007)	<0.005 ---	<0.001 ---	2.15
Ni-Cr	**WQ**	69.53 (67.97)	30.46 (31.98)	<0.01 ---	<0.01 ---	<0.01 ---	<0.01 ---	<0.01 ---	<0.01 ---	0.010 (0.045)	0.001 (0.003)	<0.005 ---	0.001 (0.002)	2.13
Ni-Cr	**FC+10% CW**	68.91 (67.99)	30.42 (31.94)	<0.01 ---	0.01 (0.01)	0.02 (0.0012)	0.01 (0.011)	<0.01 ---	<0.01 ---	0.005 (0.023)	0.003 (0.010)	<0.005 ---	<0.001 ---	2.13
Ni-Cr	**FC+20% CW**	69.55 (68.01)	30.40 (31.92)	<0.01 ---	<0.01 ---	0.02 (0.0012)	0.01 (0.011)	0.01 (0.019)	<0.01 ---	0.003 (0.014)	0.003 (0.010)	<0.005 ---	<0.001 ---	2.13
Ni-Cr-1Fe	**FC**	68.51 (66.98)	30.53 (32.05	0.95 (0.93)	<0.01 ---	<0.01 ---	<0.01 ---	<0.01 ---	<0.01 ---	0.007 (0.032)	0.001 (0.003)	<0.005 ---	0.001 (0.002)	2.09
Ni-Cr-1Fe	**WQ**	68.09 (66.55)	30.94 (32.47	0.96 (0.94)	<0.01 ---	<0.01 ---	<0.01 ---	<0.01 ---	<0.01 ---	0.008 (0.036)	0.001 (0.003)	<0.005 ---	0.001 (0.002)	2.05
Ni-Cr-1Fe	**FC+10% CW**	68.57 (67.06)	30.38 (31.90)	1.01 (0.99)	<0.01 ---	0.02 (0.0012)	0.02 (0.023)	<0.01 ---	<0.01 ---	0.002 (0.009)	0.002 (0.007)	<0.005 ---	<0.001 ---	2.10
Ni-Cr-1Fe	**FC+20% CW**	68.26 (66.74)	30.70 (32.23)	1.01 (0.99)	<0.01 ---	0.02 (0.0012)	0.01 (0.011)	<0.01 ---	<0.01 ---	0.003 (0.014)	0.002 (0.007)	<0.005 ---	<0.001 ---	2.07
Ni-Cr-3Fe	**FC**	67.38 (65.91)	29.65 (31.15)	2.96 (2.90)	<0.01 ---	<0.01 ---	<0.01 ---	<0.01 ---	<0.01 ---	0.009 (0.041)	0.002 (0.007)	<0.005 ---	0.001 (0.002)	2.12
Ni-Cr-3Fe	**WQ**	66.05 (65.73)	29.86 (31.36)	2.92 (2.86)	<0.01 ---	<0.01 ---	<0.01 ---	<0.01 ---	<0.01 ---	0.010 (0.045)	0.003 (0.010)	<0.005 ---	<0.001 ---	2.10
Ni-Cr-3Fe	**FC+10% CW**	67.59 (66.15)	29.41 (30.91)	2.96 (2.90)	<0.01 ---	0.02 (0.0012)	0.01 (0.011)	<0.01 ---	<0.01 ---	0.003 (0.014)	0.003 (0.010)	<0.005 ---	<0.001 ---	2.14
Ni-Cr-3Fe	**FC+20% CW**	68.22 (66.78)	28.96 (30.44)	2.78 (2.72)	<0.01 ---	0.02 (0.0012)	0.01 (0.011)	<0.01 ---	<0.01 ---	0.004 (0.018)	0.003 (0.010)	<0.005 ---	<0.001 ---	2.19
Ni-Cr-5Fe	**FC**	66.05 (64.62)	29.38 (30.86)	4.55 (4.45)	<0.01 ---	<0.01 ---	<0.01 ---	<0.01 ---	<0.01 ---	0.009 (0.041)	0.006 (0.020)	<0.005 ---	0.001 (0.002)	2.09
Ni-Cr-5Fe	**WQ**	63.12 (62.03)	31.22 (33.09)	4.93 (4.82)	<0.01 ---	<0.01 ---	<0.01 ---	<0.01 ---	<0.01 ---	0.009 (0.041)	0.005 (0.017)	<0.005 ---	0.001 (0.002)	1.87
Ni-Cr-5Fe	**FC+10% CW**	66.32 (64.92)	28.86 (30.34)	4.75 (4.65)	<0.01 ---	0.02 (0.0012)	0.01 (0.011)	0.02 (0.039)	0.01 (0.003)	0.004 (0.018)	0.003 (0.010)	<0.005 ---	<0.001 ---	2.14
Ni-Cr-5Fe	**FC+20% CW**	65.40 (63.99)	29.74 (31.25)	4.80 (4.70)	<0.01 ---	0.02 (0.0012)	0.01 (0.011)	0.01 (0.019)	0.02 (0.006)	0.002 (0.009)	0.003 (0.010)	<0.005 ---	<0.001 ---	2.05
Ni-Cr-7Fe	**FC**	63.22 (61.84)	29.83 (31.33)	6.93 (6.78)	<0.01 ---	<0.01 ---	<0.01 ---	<0.01 ---	<0.01 ---	0.008 (0.036)	0.005 (0.017)	<0.005 ---	0.001 (0.002)	1.97
Ni-Cr-9Fe	**FC**	63.51 (61.78)	28.87 (30.34)	8.00 (7.83)	<0.01 ---	<0.01 ---	<0.01 ---	<0.01 ---	<0.01 ---	0.007 (0.032)	0.003 (0.010)	<0.005 ---	0.001 (0.002)	2.04

[1]Composition determined by CAP-017M (ICP-AES) and ASTM E 1019-11 (Comb./IGF) unless otherwise noted. [2]Co, Mn, and Mo were determined to be < 0.01 wt.%.
[3]Determined by combustion-infrared absorbance. [4]Determined by inert gas fusion-infrared absorbance. [5]FC = Furnace Cool, WQ = Water Quench, CW = cold worked by rolling

Table 1: Compositions of the Ni-Cr and Ni-Cr-Fe Alloys Investigated.

Alloy	Condition[5]	Wt.% (At.%) [1, 2]												Atomic Ni:Cr
		Ni	Cr	Fe	Mo	Nb	Ti	Si	Mn	C[3]	O[4]	P	S[3]	
Low Si	WQ	68.64 (67.07)	31.34 (32.88)	<0.01 ---	<0.01 ---	<0.01 ---	<0.01 ---	0.01 (0.02)	<0.01	<0.01 ---	0.007 (0.024)	<0.005 ---	0.001 (0.002)	2.04
High Si	WQ	68.99 (67.26)	30.58 (32.01)	0.05 (0.05)	<0.01 ---	<0.01 ---	0.04	0.28 (0.54)	<0.01	0.01 (0.045)	<0.005 ---	<0.005 ---	0.002 (0.003)	2.10
Low Mn	WQ	69.31 (67.75)	30.64 (32.16)	0.01 (0.01)	<0.01 ---	<0.01 ---	<0.01 ---	<0.01 ---	0.02	0.01 (0.045)	0.005 (0.017)	<0.005 ---	0.002 (0.003)	2.11
High Mn	WQ	69.27 (67.71)	30.52 (32.04)	0.01 (0.01)	<0.01 ---	<0.01 ---	<0.01 ---	<0.01 ---	0.19	0.01 (0.045)	<0.005 ---	<0.005 ---	0.002 (0.003)	2.11
Low Nb	WQ	68.60 (67.11)	31.09 (32.66)	<0.01 ---	<0.01 ---	0.30 (0.18)	<0.01 ---	<0.01 ---	<0.01	0.01 (0.045)	<0.005 ---	<0.005 ---	0.003 (0.005)	2.05
High Nb	WQ	68.74 (67.91)	28.86 (30.62)	0.01 (0.01)	<0.01 ---	2.38 (1.41)	<0.01 ---	<0.01 ---	<0.01	0.01 (0.046)	<0.005 ---	<0.005 ---	0.001 (0.002)	2.22
Low Mo	WQ	69.04 (67.56)	30.67 (32.23)	0.01 (0.01)	0.27 (0.15)	<0.01 ---	<0.01 ---	<0.01 ---	<0.01	0.01 (0.046)	<0.005 ---	<0.005 ---	0.002 (0.003)	2.09
High Mo	WQ	67.86 (67.02)	29.60 (31.39)	0.01 (0.01)	2.47 (1.42)	<0.01 ---	<0.01 ---	0.01 (0.02)	<0.01	0.01 (0.046)	<0.005 ---	<0.005 ---	0.002 (0.003)	2.04
Mn + Si	WQ	68.72 (66.96)	30.76 (32.19)	<0.01 ---	<0.01 ---	<0.01 ---	<0.01 ---	0.32 (0.62)	0.19	0.01 (0.045)	<0.005 ---	<0.005 ---	0.001 (0.002)	2.08
Model A690	WQ	62.70 (61.21)	28.00 (29.35)	8.79 (8.58)	<0.01 ---	<0.01 ---	<0.01 ---	0.31 (0.60)	0.18	0.01 (0.045)	0.01 (0.034)	<0.005 ---	0.001 (0.002)	2.09
Model 52i	WQ	63.87 (63.09)	28.28 (30.00)	2.56 (2.53)	<0.01 ---	2.43 (1.44)	<0.01 ---	0.01 (0.02)	2.83	0.01 (0.046)	0.009 (0.031)	<0.005 ---	0.002 (0.003)	2.10

[1]Composition determined by CAP-017M (ICP-AES) and ASTM E 1019-11 (Comb./IGF) unless otherwise noted. [2]Co, Mn, and Mo were determined to be < 0.01 wt.%.
[3]Determined by combustion-infrared absorbance. [4]Determined by inert gas fusion-infrared absorbance. [5]FC = Furnace Cool, WQ = Water Quench, CW = cold worked by rolling

Table 2: Compositions of the Ni-Cr-X Alloys Investigated.

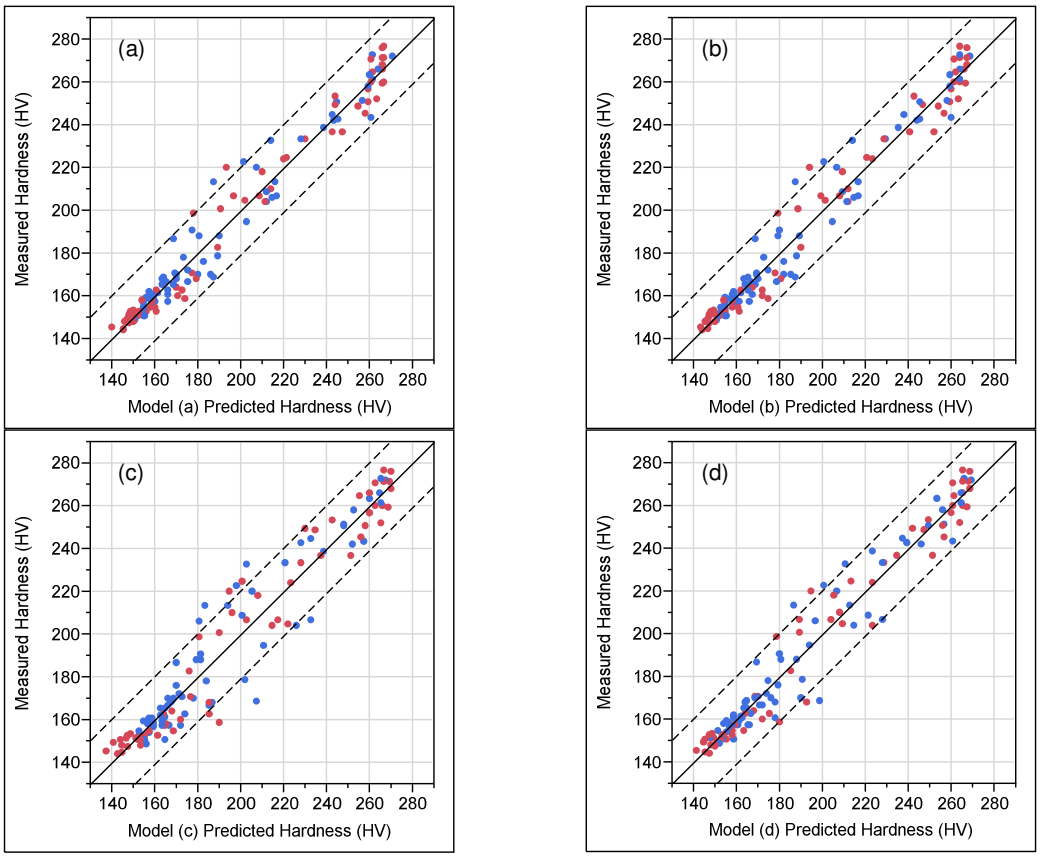

Figure 4. Actual vs. predicted hardness plots for the models considered: (a) all parameters adjustable, (b) a single *n*, (c), a single *n* and *Q*, and (d) the model chosen with two *Q*'s (one for furnace cooled (red points) and one for water quenched (blue points) samples) and a single *n*. The dashed represent two-sigma (~95% coverage) intervals, using the standard deviation from the preferred model (d).

Ni-Cr-Fe Alloys

The effects of alloying with iron are presented in Figure 6. In Figure 6, the trend lines are from the furnace cooled and water quenched binary alloys for comparison. As shown, for low concentrations of iron (1 and 3 atomic %), alloying has little effect on the hardening and the data are well fit by the binary trend lines. However, alloys with ≥ 5 atomic % iron, the highest ageing temperature show very different behavior. For example, consider the Ni_2Cr+7Fe furnace cooled samples. That alloy shows no hardening at 470°C up to 10,000 hours, somewhat delayed hardening at 418°C but 'normal' (binary alloy rate) hardening at 373°C. This delay or lack of hardening is also seen in the Ni_2Cr+5Fe and Ni_2Cr+9Fe samples, indicating that iron has shifted the time-temperature-transformation kinetics of LRO, in agreement with previous work and the research of Frely et al. [8, 20, 21]. It is an important point to note that the Ni_2Cr+9Fe alloy *does harden* (i.e., iron does not impart immunity to LRO) but only hardens at lower temperatures.

In addition to the current study, data from the literature on both model and selected commercial alloys are presented in Figure 7, which summarizes the effect of iron on the stability of the ordered phase. In Figure 7, filled points are temperatures where long range order has been observed, shaded points indicate some hardening or short range order, while open points represent stability of the disordered alloy [20, 21]. As shown by the black trend line, iron acts to lower the temperature below which the ordered phase is stable. Note also the data plotted for Alloy 690 with two different iron levels (blue points). One low iron variant (7.2 wt.% Fe) has been confirmed to show LRO at 420°C, while the normal iron alloy (10.4 wt.%) is above the regime of Ni_2Cr stability at 420°C. Lower temperature ageing have produced some hardening but no direct evidence of long range order to date [6].

Figure 8 shows data for the furnace cooled Ni_2Cr-3Fe alloy with 10% (left hand plot) and 20% (right hand plot) cold work. Again, the dashed lines represent best fits from the non-cold worked binary alloy for comparison. The data are fairly well described by the trend lines for the non-cold worked alloy but the significant softening that occurs at time ≥ 100 hours confounds detailed analyses of these data. As mentioned previously, the cold worked data were excluded from the statistical fitting of the KJMA equation because of this softening.

The data in Figure 7 are used in conjunction with the apparent activation energies for LRO and the hardness data to estimate time-temperature-transformation (TTT) diagrams as a function of iron content. In Figure 9, the horizontal dashed line represents the temperature above which the ordered phase in unstable (from the dashed line in Figure 7), while the curved line represents a temperature dependence of 147 kJ/mol for the water quenched alloys and 244 kJ/mol for the furnace cooled alloys. Where available, the hardness data are plotted on the graphs in two groups: X's represent potential hardening due to LRO (+10 to +20 increase in Vicker's hardness) and the square representing a hardness increase of ≥20 HV, which is judged to be a good indicator of a significant degree of ordering. The plots are presented from 1 at.% to 11 at.% Fe, using the same methodology (even though there are only data to 9 at. % Fe for the FC condition and 5 at.% Fe for the WQ condition). Based on the hardness data, the temperature dependent curves are anchored to bound the ≥20 HV data as a reasonable 'start' to the TTT curve for LRO.

Consider the Ni-Cr-9Fe plot for the furnace cooled alloy in Figure 9. This graph is relevant to Alloy 690, which is near Ni_2Cr stoichiometry, contains a minimum of 9 wt.% iron, and it typically used in annealed and thermally treated conditions that are likely in thermal equilibrium with respect to the vacancy concentration. The maximum temperatures relevant to PWR systems would be ~345°C (pressurizer), 325°C (primary coolant) and 285°C (secondary coolant) [22]. The predicted times at which LRO may begin to occur are summarized in Table 3. For the furnace cooled material (likely relevant to most wrought Alloy 690), there is no concern for LRO at steam generator temperatures but real concern that primary or pressurizer components could develop LRO in-service. The onset of hardening should take >1 year at 345°C, and >6 years at 325°C for furnace cooled material. Higher iron concentrations would shift this onset to longer times, while excess vacancies (possibly present from welding thermal cycles or irradiation damage) should accelerate the onset. However, as will be discussed in more detail below, available data suggest that the development of LRO is even more sluggish than these estimates, indicating that other alloying elements affect the TTT kinetics.

Temperature	Ni-Cr-9Fe Furnace Cooled ($Q_{Apparent}$ = 244 kJ/mol)	Ni-Cr-9Fe Water Quenched ($Q_{Apparent}$ = 147 kJ/mol)
345°C / 653°F (Pressurizer)	>10,000 hours (>1 year)	>2,000 hours (> 3 months)
325°C / 617°F (Primary Coolant)	>50,000 hours (>6 years)	>6,000 hours (>8 months)
285°C / 545°F (Secondary Coolant)	>1,000,000 hours (>114 years)	>80,000 hours (>9 years)

Table 3: Estimates of minimum times for the onset of hardening due to Ni_2Cr formation for a Ni_2Cr-9 at.% Fe alloy (near Alloy 690) in the furnace cooled and water quenched conditions.

Ni-Cr-X and more Complex Alloys

The effects of common alloying elements other than iron are summarized in Figure 10. In Figure 10, the baseline binary water quenched data are shown on the bottom left, and the curve fits to these data (dashed lines) are reproduced on all of the plots in order to facilitate comparison. Data to the left of the corresponding dashed line indicate faster ordering kinetics, while data to the right of the corresponding line indicate delayed kinetics.

The first two rows show the effects of the 'low' and 'high' levels of silicon (0.01 and 0.28 wt.%), manganese (0.02 and 0.19 wt.%), niobium (0.30 and 2.38 wt.%), and molybdenum (0.27 and 2.47 wt.%). As shown, the 'low' levels of alloying elements have little effect on the hardening kinetics as the data fall reasonably close to the binary alloy trend lines. At the 'high' levels though, it appears that molybdenum may accelerate the ordering kinetics, at least at 470°C (878°F) and 418°C (784°F), since the data are consistently shifted to shorter times relative to the trend lines. This result is consistent with the work of Karmazin et al., who also reported that molybdenum shifted the C-curve for LRO to higher temperatures and shorter times at 560°C (Ni-24Cr-8Mo) but appeared to delay LRO by ~10X at 450°C [23]. In addition to Mo, some of the high Nb 418°C (784°F) ageing appear to be spuriously fast or hard (e.g. the 3000 hr data point). In an Nb-bearing alloy, hardening by γ'' is a possibility but this should occur at both 470°C and 418°C if it is influencing the hardness of the samples, and the 470°C do not appear to show anomalous hardening. Additional work is needed to characterize the microstructure of these samples.

The combination of Mn+Si at typical levels found in Alloy 690 is shown in the bottom row (second plot from the left on Figure 10). As shown, the data are fairly well fit by the binary data. The 418°C (784°F) data are somewhat accelerated relative to the binary alloy trend line, but unlike the molybdenum data, this not observed at higher temperatures, suggesting this may be scatter in the data. These data show that Mn+Si do not, by themselves, delay the development of LRO in Alloy 690.

Lastly, 'model' versions of two industrial alloys, EN52i weld metal and Alloy 690 are shown in the bottom right of Figure 10. Note that this is somewhat of an overtest of EN52i, since the chromium level is a little high relative to the commercial alloy to maintain a 2:1 nickel:chromium ratio (actual EN52i has Ni:Cr of 2.2:1.0). EN52i is of interest because, while low in iron, it is rich in other alloying elements (e.g. Mn and Nb), and appears to be resistant to LRO. As shown for times up to 3000 hours, there is no increase in hardness. Similarly, the model Alloy 690 does not show hardening at times up to 3000 hours. This is in contradiction to Figure 9, which indicates that for both a 3 at.% Fe WQ and 9 at.% WQ alloy (i.e., near the Model EN52i and Alloy 690 compositions), there should be appreciable hardening. Apparently, ordering kinetics are not a simple function of the iron content but may depend significantly on the total alloy content.

The complexities of alloying element effects are further highlighted by a review of reports of ordering in engineering alloys. Literature reports of ordering in several Ni-Cr alloys are summarized in Table 4. In Table 4, the alloys are listed from highest chromium concentration to the lowest, with columns for the major alloying elements, Ni:Cr ratio, ageing time and temperature, degree of cold work, and notes on the research. Alloys that have been reported to show long range order are marked by the dark shading, alloys with potential ordering (e.g. hardening but no confirmation of LRO) are given a lighter shading, while alloys with no ordering for the given time and temperature are left with a white background.

As shown, a wide range of alloys with varying stoichiometry (Ni:Cr of 3.9-1.8) have been reported to show LRO. Many of the alloys shown to exhibit LRO contain molybdenum, consistent with its reported effects of increasing the high temperature kinetics and widening the compositional range of phase stability [23]. It is tempting to compare the alloys based on the (Ni:(Cr+Mo)) ratio, since both Cr and Mo are bcc elements, but research by Karmazin suggests that Mo substitutes for both Ni and Cr in the Ni_2Cr structure. The alloy data that exhibit hardening are shown relative to a recent Ni-Cr phase diagram adapted from Xiong in Figure 11 [3]. That figure further supports the notion that Mo widens the Ni_2Cr phase field in terms of both temperature and compositions.

Note that in Table 4, the data for Alloy 690 (or slightly low iron variants) are mixed [2, 6, 20, 21, 24]. LRO has been confirmed in a low iron heat (7.2 wt.%) but in-specification alloys have only shown hardening, not true long range order for exposure times out to 90,000 hours. These data are also shown in Figure 12a, which attempts to summarize data for near Alloy 690 compositions and to draw a tentative time-temperature-transformation (TTT) curve. As shown in Figure 12a., there is some discrepancy near the 'tails' of the curve where lower Fe alloys show hardening but the higher iron alloys do not, at least for the ageing times reported to date.

Figure 12b reproduces the TTT curve from 12a and illustrates some significant metallurgical effects. Iron additions act to decrease the temperature below which the ordered phase is stable, effectively shifting the C-curve down and to the right relative to the binary alloy. In contrast, this work and literature data indicate that molybdenum stabilizes the ordered phase at higher temperatures and may accelerate LRO by shifting the nose of the C-curve to higher temperatures and shorter times. Heat treatments like water quenching, or potentially irradiation damage to produce excess vacancies, can accelerate the development of long range order by lowering the apparent activation energy (driving the start of the transformation to shorter times). Cold work can act to delay the onset of ordering, likely by destroying any short or long range order that can form on slow cooling.

Despite the limited data, the methodology outlined in Figure 9 and summarized in Figure 12 to estimate a reasonable TTT diagram for Alloy 690 can be used to help gauge the level of concern for light water reactor systems. These estimates are based on isothermal data and do not consider any potential accelerating effects (e.g. irradiation damage, alloying with Mo or tensile stress). The time scales of interest are ~3.5×10^5–5.2×10^5 hours (40-60 years at temperature). As shown, hardening due to LRO is not expected below 300°C for any system, indicating that Ni-Cr components in boiling water reactor and the steam generating system of pressurized water reactors are of little concern. At pressurized water reactor primary plant temperatures (~≤325°C), there is also small concern, since the transformation start is expected ~40 years. However, for the pressurizing system (T~≤345°C), the tentative TTT diagram indicates reasonable concern, with the start of hardening due to LRO predicted to occur ~80,000 hours (~ 9 years).

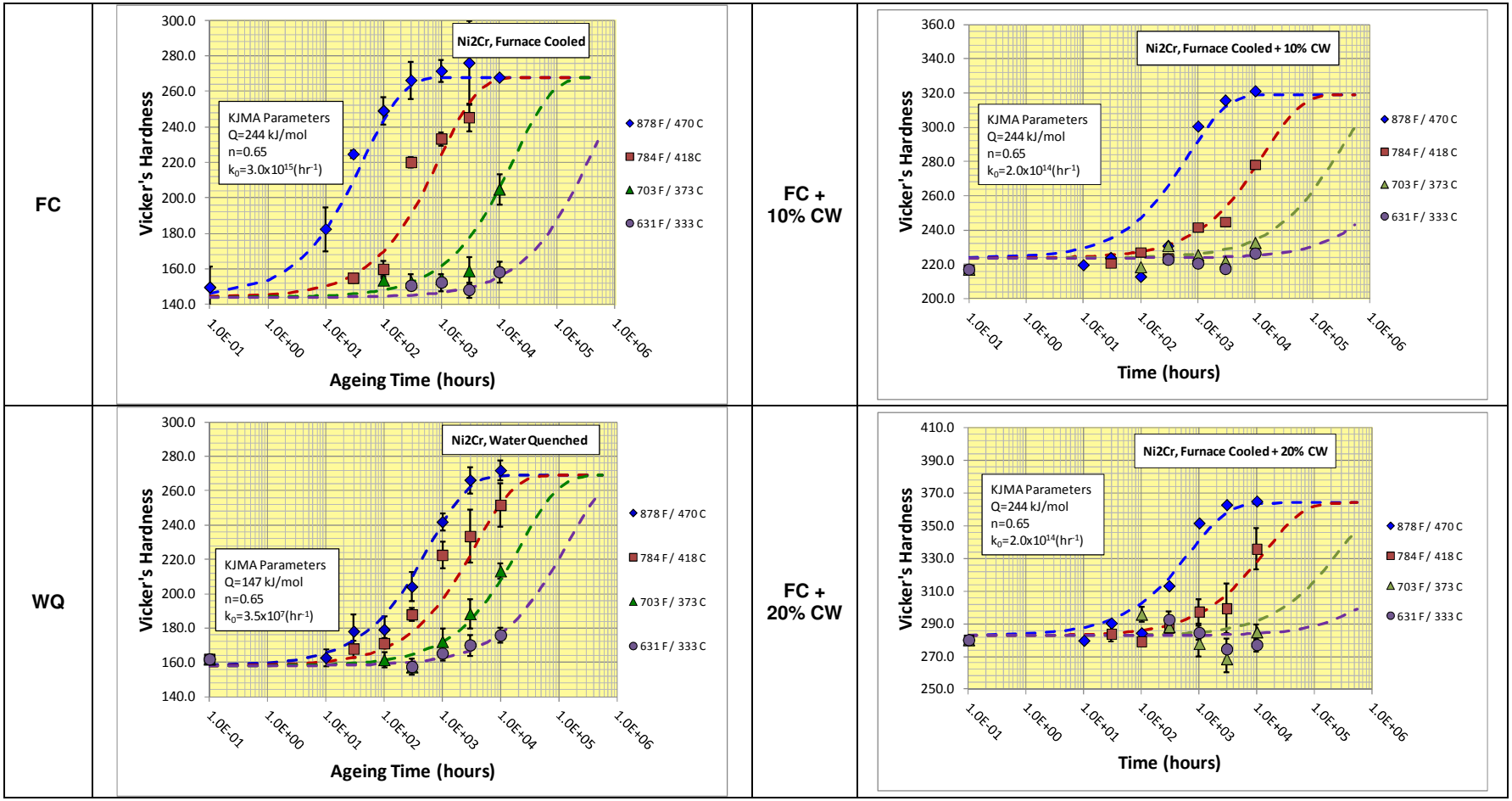

Figure 5: Results from the Ni-Cr binary alloys. The alloys were all well fit with an Avrami exponent ~0.65 indicating asymmetrical diffusional growth but with different temperature dependence and prefactors. The water quenched alloy displayed a relatively low apparent activation energy (~147 kJ/mol, indicative of vacancy migration control) relative to the furnace cooled alloys (Q~244 kJ/mol suggest bulk diffusional growth). Cold work did not affect the activation energy but appears to delay the onset of ordering relative to the furnace cooled (FC) alloy). Note that the same set of parameters well fit the 10% and 20% cold worked material. The error bars represent the range of individual measurements, with five hardness indents per condition.

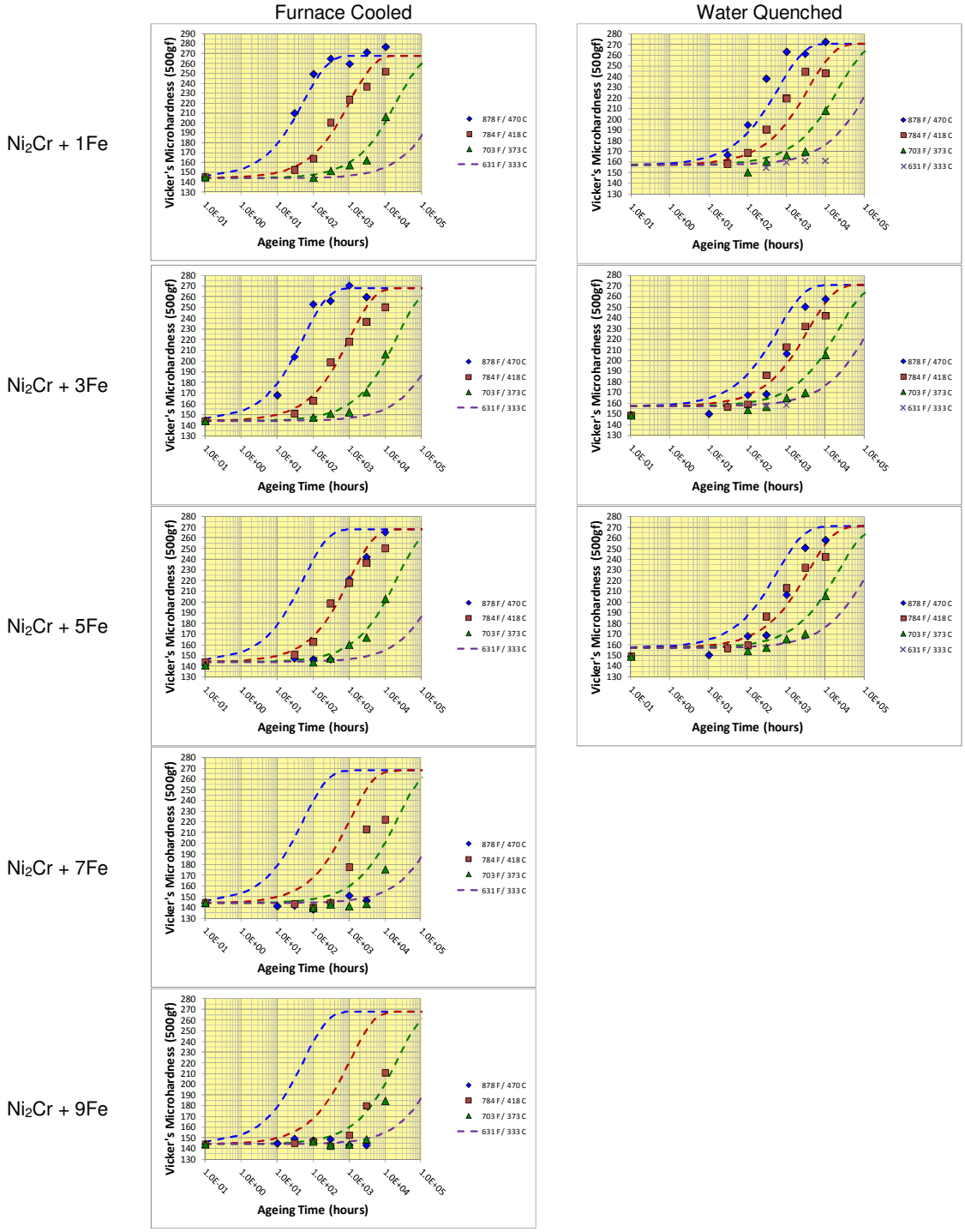

Figure 6: Effect of iron additions on the hardening from long range ordering. The 1at.% Fe and 3 at.% Fe alloys show relatively well behaved hardening but at 5 at.% Fe, the highest temperature ageing (470°C) show slower hardening rates, suggesting the 'nose' of the time-temperature-transformation curve has shifted. Similarly, at 7 at.% and 9 at.% Fe, the 470°C aged data show no sign of hardening and the 418°C data are delayed.

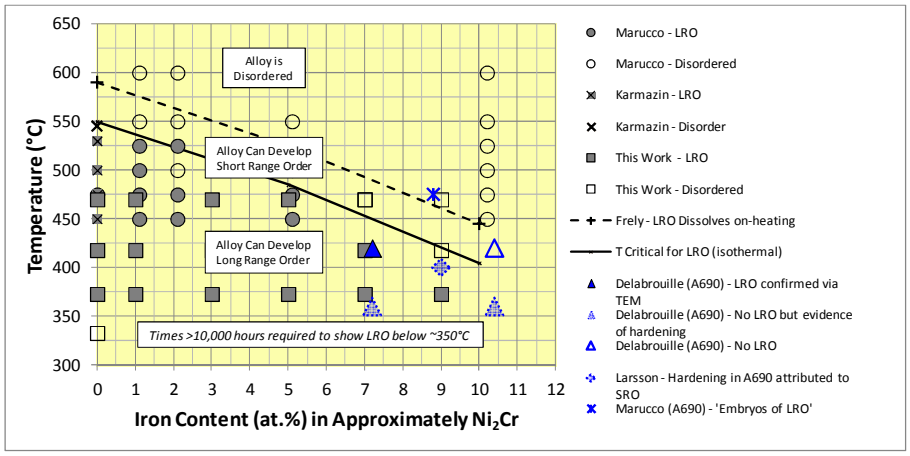

Figure 7: Illustration of the effect of iron on the temperature below which the Ni_2Cr phase is stable.

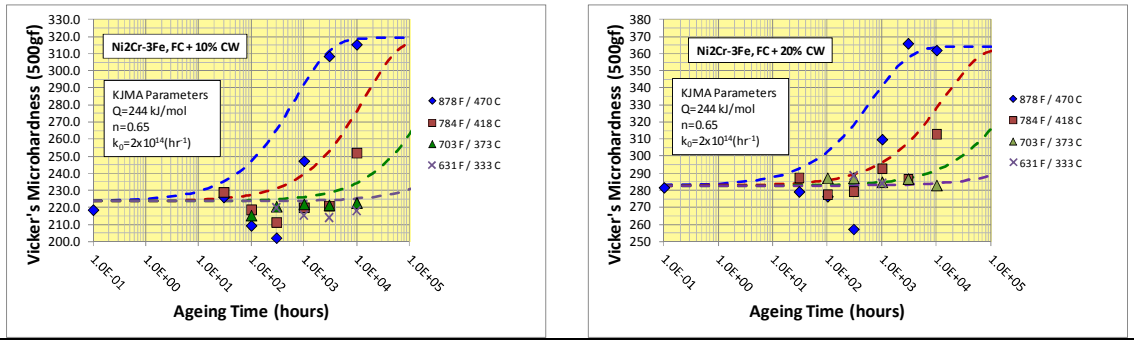

Figure 8. Data for 10% and 20% cold worked Ni_2Cr-3Fe. Note the softening at the higher ageing temperatures that confounds fitting of the KJMA equation.

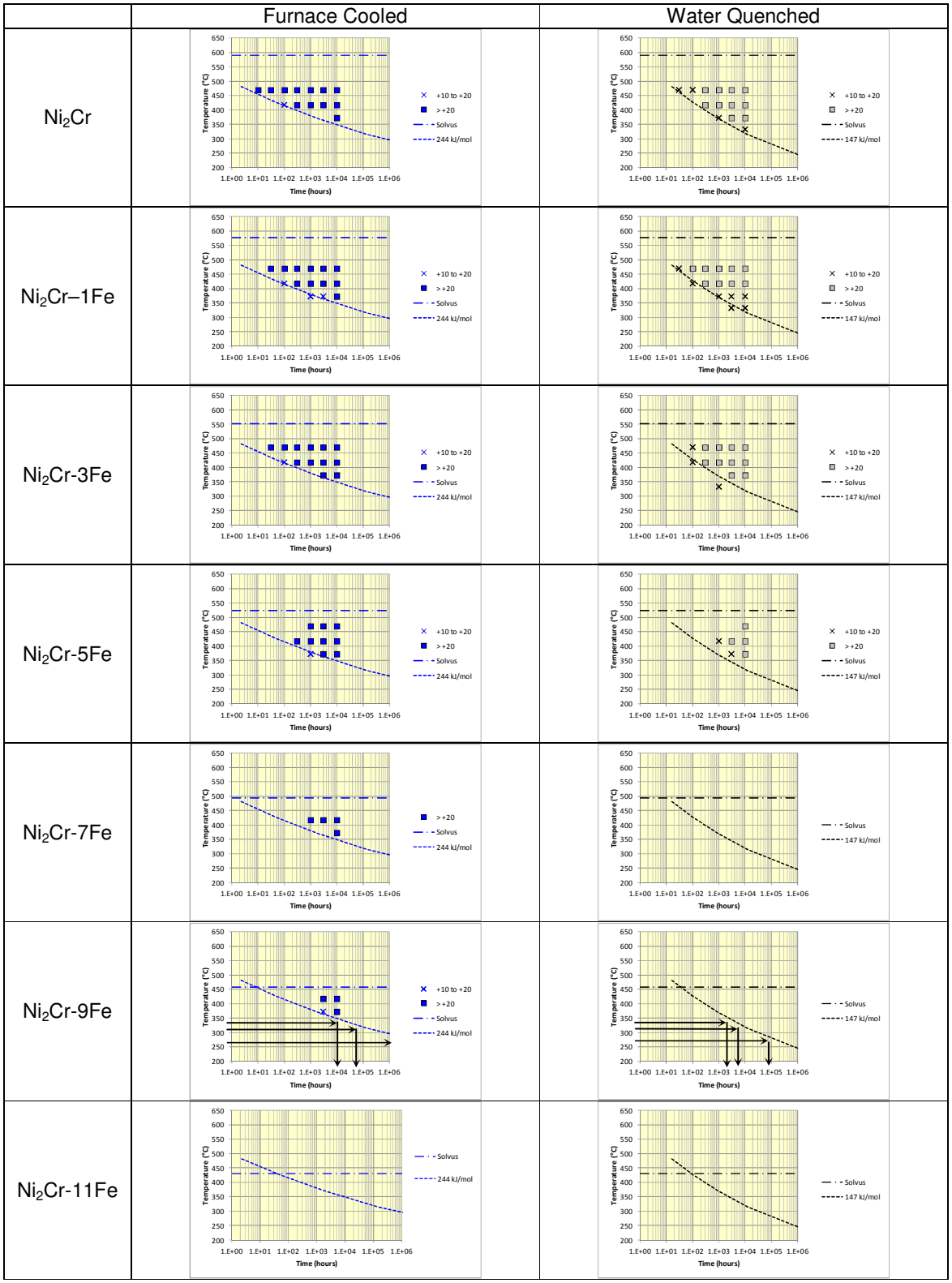

Figure 9. Summary data for the onset of hardening due to ordering as a function of iron concentration. The upper temperature limit (dash-dot line) and a kinetic limit anchored to bound the data (dashed line) are shown for illustration.

	Ni_2Cr + Si	Ni_2Cr + Mn	Ni_2Cr + Nb	Ni_2Cr + Mo
'Low' Level	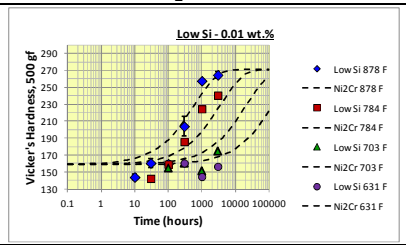	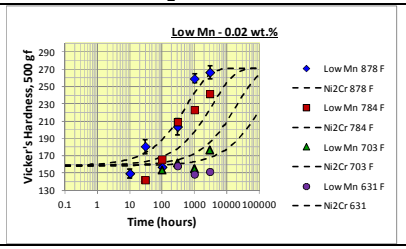	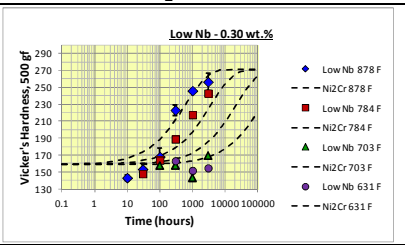	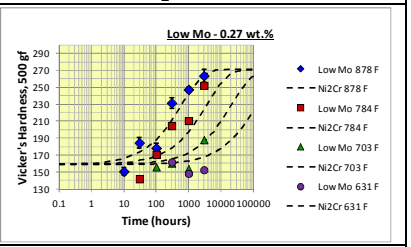
'High' Level	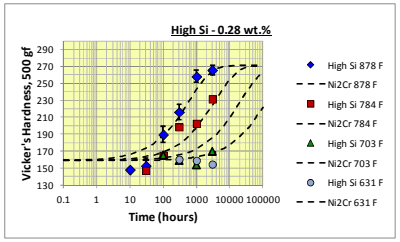	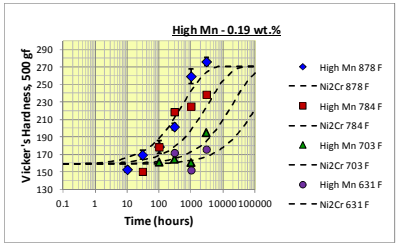	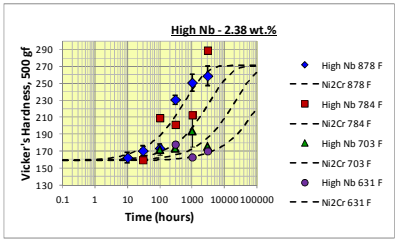	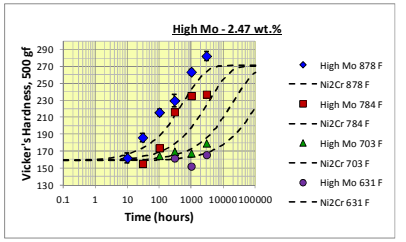
	Ni_2Cr Binary	Ni_2Cr + Mn + Si	Model 52i	Model A690
Ni2Cr and Complex Alloys	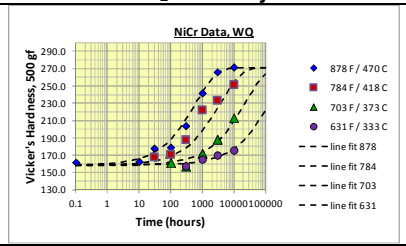	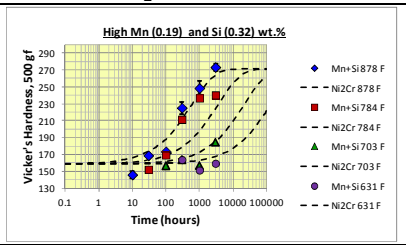	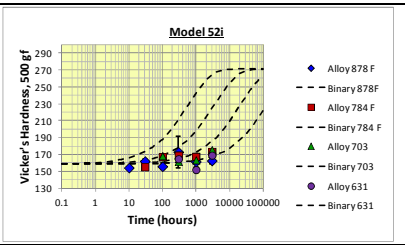	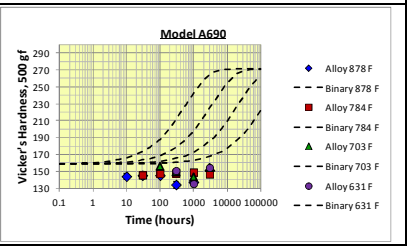

Figure 10. Illustration of the effects of various alloying elements on the kinetics of hardening due to long range order. The dashed lines are for the binary alloy in each graph. The high molybdenum alloy shows somewhat faster hardening at the two highest ageing temperatures.

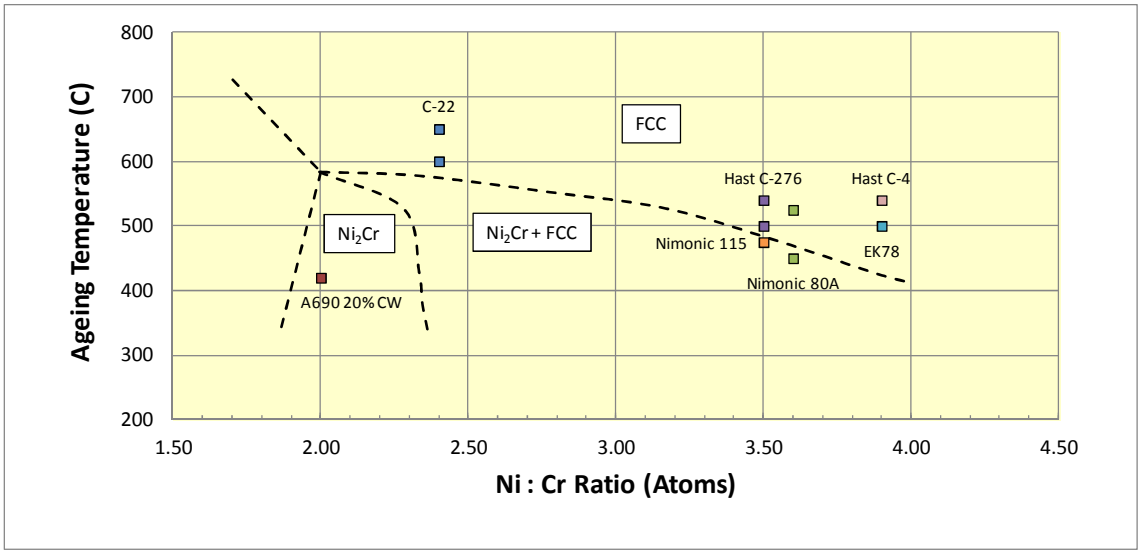

Figure 11. Illustration of where some engineering alloys reported to show long range ordering are relative to a recent Ni-Cr phase diagram, adapted from Xiong [3].

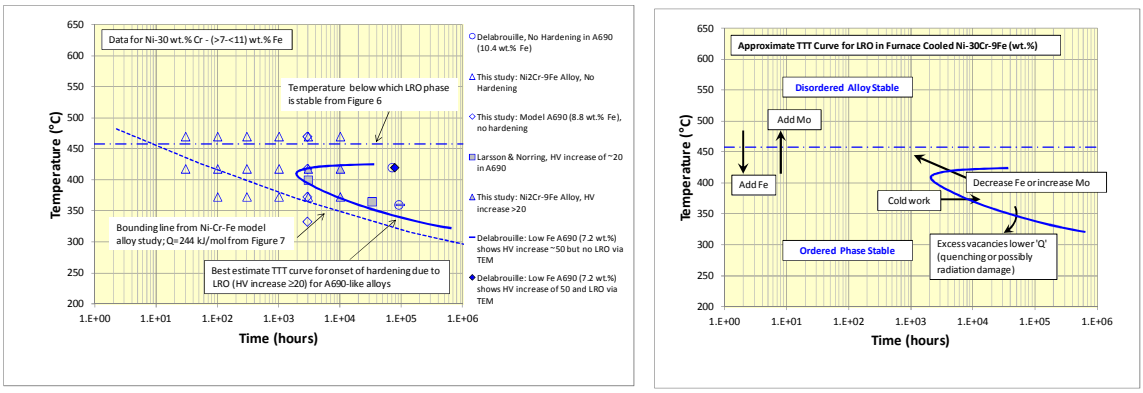

Figure 12. a.) Summary data for alloys near the A690 composition along with a tentative TTT curve (solid blue line) and b.) a schematic of how different metallurgical factors affect the TTT kinetics of LRO.

Conclusions

- The hardening due to the development of LRO in Ni-Cr alloys is well fit by KJMA kinetics with an exponent near 0.65 and a activation energy of either 244kJ/mol for furnace cooled alloys or 147 kJ/mol for water quenched alloys.
- Cold work delays the onset of ordering in furnace cooled alloys but has no discernible effect on the apparent activation energy or the Avrami exponent.
- Alloying additions of iron lower the temperature below which the ordered phase is stable but do not appear to influence either the activation energy or the Avrami growth exponent.
- Alloying with molybdenum (2.47 wt.%) accelerates ordering at temperatures of 470°C and 418°C but apparently, not at lower temperatures. Other alloying additions investigated (Si, Mn, Nb, and Mn+Si) do not have significant effects on the hardening kinetics attributed to LRO. However, more complex alloys like Alloy 690 and EN52i may be more resistant to hardening relative to its simplified model alloy counterpart (e.g. A690 vs. Ni-30Cr-9Fe).
- Engineering alloys reported to display long range order possess a wide range of compositions, suggesting a large phase field of stability that may be increased in temperature and/or composition by alloying with molybdenum.
- An approximate TTT diagram for alloys near the A690 composition indicates that hardening and LRO can occur at times and temperatures of interest to pressurized water reactors. However, for Ni-30Cr-9Fe alloys (i.e., near Alloy 690), in the absence of some other accelerating effect, (e.g. irradiation damage), only components exposed to >325°C (i.e., the pressurizing system) are expected to be of concern, based on a 40 year time at temperature lifetime.

Acknowledgements

The Authors are indebted to Mr. Joe Badalucco who performed all of the microhardness testing, Dr. Robb Morris for the SEM examinations, and Mr. Nathan Lewis for the TEM analyses.

Researcher	Alloy	Cr wt.%	Fe wt.%	Mo wt.%	Co	Ni:Cr Atoms	Cold Work	Ageing Temp (°C)	Ageing Time (hrs)	LRO ?	Notes
Delabrouille [6]	A690	30.7	10.4	0	0	1.8	20%	360	90,000	No	But increase of ~50 HV 5 at 90,000 hrs
		30.7	10.4	0	0	1.8	20%	420	70,000	No	But increase of ~25 HV 5 at 70,000 hrs
		30.7	10.4	0	0	1.8	0%	360	90,000	No	No hardening
		30.7	10.4	0	0	1.8	0%	420	70,000	No	No hardening
Larsson [24]		30.0	10.0	0	0	1.8	0%	400	3000	See Note	HV 0.5 increase ~20 HV from 168 to 178, no evidence of LRO via TEM
Norring [24]		30.0	10.0	0	0	1.8	0%	365	32,961	See Note	Hardness increase ~21 HV from HV 178 to 199, no evidence of LRO via TEM
Frely [20, 21]		30	10	0	0	1.8	0%	300-500	?	No	Relatively short times ?
Delabrouille [6]		29.0	7.2	0	0	2.0	20%	360	90,000	No	But increase of ~50 HV 5 at 90,000 hrs
		29.0	7.2	0	0	2.0	20%	420	70,000	Yes	Confirmed by TEM Increase ~50 HV
		29.0	7.2	0	0	2.0	0%	360	90,000	No	But increase of ~50 HV 5 at 90,000 hrs
		29.0	7.2	0	0	2.0	0%	420	70,000	Yes	Confirmed by TEM increase ~50 HV
Marucco [2]		29.0	8.8	0	0	1.8	0%	475	30,000	See Note	TEM indicates start of ordering
Young - This Work		29.0	9.0	0.2	0		0%	333-470	3,000	No	Model alloy
Mukherjee [25]	A625	21.7	3.9	8.8	0	2.7	0%	600	60,000	Yes	
Edgecumbe [26]	C-22	21.1	4.7	13.5	0	2.4	0%	600-650	100 - 1000	Yes	
Xie [27]	C-22HS	21.0	2.0	17.0	0	2.6	0%	593	16,000	Yes	Alloy designed to strengthen via ordering
Metcalf [4]	Nimonic 80A	19.5	0.5	0	0.5	3.6	0%	450-525	1,000 - 30,000	Yes	Elastic tensile strain may accelerate ordering
Marucco [2]		19.5	0.8	0	0.4		0%	475	20,000	Yes	Based on lattice contraction
Larsson	Hastelloy C-276	16.0	6.5	15.0	0		0%	500	1,000	Yes	Confirmed by TEM
Gdowski / Tawancy [28]		15.5	5.5	16.0	0	3.5	0%	540	~1,000	Yes	
Gdowski / Tawancy [28]	Hastelloy C-4	16.0	1.0	15.5	0	3.9	0%	540	~1,000	Yes	
Goman'kov [29]	EK78	15.6	0.0	4.3	5.6	3.9	0%	500	5,000	Yes	500°C was last phase of complex heat treatment
Marucco [2]	Nimonic 115	15.0	1.0	4	14.0	3.5	0%	475	20,000	Yes	Based on lattice contraction
Marucco [2]	Nimonic 105	14.8	1.0	5	20.0	3.3	0%	475	20,000	Yes	Based on lattice contraction

Table 4: Ni-Cr based engineering alloys and time/temperature conditions reported to exhibit long range order (dark shading), potential ordering (light shading), and no ordering (white background).

References

1. Nash, P., *Phase diagrams of binary nickel alloys*. 1991, Materials Park, OH: ASM International.
2. Marucco, A., G. Carcano, and E. Signorelli. *Consequences of Ordering on the Structural Stability of Ni Base Superalloys*. in *Materials Ageing and Component Life Extension*. 1995. Milan, Italy.
3. Xiong, W., *Thermodynamic and Kinetic Investigation of the Fe-Cr-Ni System Driven by Engineering Applications*, in *Materials Science and Engineering*2012, KTH Royal Institute of Technology: Stockholm, Sweden. p. 1-77.
4. Metcalfe, E., B. Nath, and A. Wickens, *Some Effects of the Ordering Transformation in Nimonic 80A on Stress Relaxation Behavior.* Mat. Sci. & Eng., 1984. **67**: p. 157-162.
5. Marucco, A., *Phase transformations during long-term ageing of Ni-Fe-Cr alloys in the temperature range 450-600 °C.* Materials Science & Engineering A: Structural Materials: Properties, Microstructure and Processing, 1995. **A194**(2): p. 225-233.
6. Delabrouille, F., et al. *Long Range Ordering of Alloy 690*. in *14th International Conference on Environmental Degradation of Materials in Nuclear Power Systems*. 2009. Virginia Beach, VA: ANS.
7. Tsutsumi, K. and T. Couvant. *Evaluation of the Susceptibility to SCC Initiation of Alloy 690 in Simulated PWR Primary Water*. in *15th International Conference on Environmental Degradation of Materials in Nuclear Power Systems - Water Reactors*. 2011. Colorado Springs, CP: TMS.
8. Young, G.A., J.D. Tucker, and D.R. Eno. *The Kinetics of Long Range Ordering in Ni-Cr and Ni-Cr-Fe Alloys*. in *16th International Conference on Environmental Degradation of Materials in Nuclear Power Systems - Water Reactors*. 2013. Asheville, NC: NACE.
9. G.A. Young, J.D.T., and D.R. Eno. *The Kinetics of Long Range Ordering in Ni-Cr and Ni-Cr-Fe Alloys*. in *16th International Conference on Environmental Degradation of Materials in Nuclear Power Systems - Water Reactors*. 2013. Asheville, NC: NACE.
10. Kolmogorov, A., *A Statistical Theory for the Recrystallization of Metals.* Akad. nauk SSSR, Izv., Ser. Matem., 1937. **1**: p. 355.
11. Johnson, W. and R. Mehl, *Reaction Kinetics in Processes of Nucleation and Growth.* Trans. AIME, 1939. **135**: p. 416.
12. Avrami, M., *Kinetics of Phase Change. I General Theory.* J. Chem. Phys., 1939. **7**: p. 1103-1112.
13. Avrami, M., *Kinetics of Phase Change. II Transformation-Time Relations for Random Distribution of Nuclei.* J. Chem. Phys., 1940. **8**: p. 212-224.
14. Avrami, M., *Kinetics of Phase Change. III Granulation, Phase Change, and Microstructures.* J. Chem. Phys., 1941. **9**: p. 177-184.
15. Criado, J.M. and A. Ortega, *Non-Isothermal Crystallization Kinetics of Metal Glasses: Simulataneous Determination of Both the Activation Energy and the Exponent n of the JMA Kinetic Law.* Acta Met., 1987. **35**(7): p. 1715-1721.
16. Marucco, A. and N. Birendra, *Effects of ordering on the properties of Ni-Cr alloys.* J. Mat. Sci., 1988. **23**(6): p. 2107-14.
17. Glicksman, M.E., *Diffusion in Solids*. 2000, New York: John Wiley & Sons.
18. Smithells, C.J., W.F. Gale, and T.C. Totemeier, *Smithells Metals Reference Book*. 2004: Elsevier Inc.
19. Berg, H. and J.B. Cohen, *Long-Range Order and Kinetics in $CoPt_3$.* Met. Trans, 1972. **3**: p. 1797-1805.
20. Frely, E., et al. *Short and Long-Range Ordering of $(Ni_{0.67}Cr_{0.33})_{1-x}$ Fe_x Alloys Under Electron Irradiation.* in *Proceedings of the Materials Research Society*. 1996. Boston, MA: MRS.
21. Frely, E., et al., *Investigation of Ordering Kinetics in Ni-Cr-Fe Alloys Under Electron Irradiation.* Annales De Physique, 1997. **22**(no3): p. C2-137 - C2-144.
22. Buongiorno, J., *Engineering of Nuclear Systems*, 2010, MIT.
23. Karmazin, L., J. Krejci, and J. Zeman, *γ Phase and Ni_2Cr-type Long Range Order in Ni-Rich Ni-Cr-Mo Alloys.* Mat. Sci. Eng., 1994. **A183**: p. 103-109.
24. Larsson, T., J.-O. Nilsson, and J. Frodigh. *On the Possibility of Forming Ordered Ni_2Cr in Alloy 690*. in *Ninth International Symposium on Environmental Degradation of Materials in Nuclear Power Systems - Water Reactors*. 1999. Newport Beach, CA: TMS.
25. Mukherjee, P., et al., *Lattice Misfit Measurement in Inconcel 625 by X-ray Diffraction Technique.*
26. Summers, T.S.E., et al., *Phase Stability and Mechanical Properties of C-22 Alloy Aged in the Temperature Range 590 to 760 Degrees C for 16,000 Hours*, 1998, LLNL.
27. Xie, X., et al., *The Precipitation and Strengthening Behavior of Ni2(Mo.Cr) in Hastelloy C-22HS Alloy, A Newly Developed High Molybdenum Ni-Base Superalloy.*
28. Gdowski, G.E., *Survey of Degradation Modes of Four Nickel-Chromium-Molybdenum Alloys*, 1991, Lawrence Livermore National Laboratory: Livermore. p. 1-67.
29. Gorman'kov, V.I., et al., *Atomic Ordering in the Phases of a Nickel-Chromium-Based Superalloy.* Russian Metallurgy, 2008. **2008**(6): p. 500-505.